

Glucose, Fructose and H₂O₂ Detection by Microstructured Copper and Cobalt Oxides Electrodeposited onto Glassy Carbon Electrodes using Potentiostatic or Potentiodynamic Methods

Ulrich Briones-Guerash Silva¹, Jorge Alberto Velásquez-Reales¹, Paola Gómez Tagle Chávez², Julio César Aguilar Cordero^{1,*}

¹ Departamento de Química Analítica, Universidad Nacional Autónoma de México, Ciudad Universitaria, Coyoacán, Ciudad de México, C.P. 04510, México

² Departamento de Química Inorgánica y Nuclear, Universidad Nacional Autónoma de México, Ciudad Universitaria, Coyoacán, Ciudad de México, C.P. 04510, México

*E-mail: julioca@unam.mx

Received: 3 May 2022/ Accepted: 31 May 2022/ Published: 7 August 2022

Copper or cobalt oxides were potentiostatically or potentiodynamically electrodeposited onto glassy carbon electrodes (GCE), and their activities in the electrooxidation of glucose, fructose and H₂O₂ were compared. Pourbaix diagrams, including acid-base, solubility, mono- and polynuclear complex formation equilibria, were calculated to evaluate the most suitable conditions for electrodeposition, which were subsequently verified by voltammetric studies. The magnitude and duration of the potential pulses, potential range, and temperature were studied to determine a maximum sensitivity toward glucose, fructose or H₂O₂. The metal oxide-modified GCE was morphologically and chemically characterized by scanning electron microscopy (SEM/SEM-EDS) and used to determine the glucose content in pharmaceutical and synthetic aqueous solutions with satisfactory results. Our simple metal oxide-modified electrodes show sensitivity values that are similar (1929.7 $\mu\text{A mM}^{-1} \text{cm}^{-2}$ for glucose using a Cu₂O/GCE) to those obtained using other, more complex modified electrode architectures reported in the literature and also show sufficiently low limits of detection ($60 < \mu\text{M}$) for eventual application in glucose analysis of real samples.

Keywords: Nonenzymatic electrodes, glucose, fructose, copper oxides, cobalt oxides

1. INTRODUCTION

Analytical methods for the analysis of sugars are very common both in medical studies and the food industry. Typical examples are fructose quantification in beverages, syrups or honey, as well as glucose analysis in human blood or urine samples.[1,2] These methods of analysis are highly relevant since they provide ways to monitor and prevent health-related issues such as diabetes.[3] Among the most common methods used for the analysis of glucose and fructose, we find those based on chromatographic techniques (GC and HPLC),[4,5] the Lane-Eynon titration and many other methods in the food industry,[6–8] while electrochemical[9] and optical[10] sensors are the most widely used for medical applications, mainly due to their selectivity and ease of use.

Hydrogen peroxide is also a very important compound from an analytic point of view since its concentration levels are related to various physiological processes (e.g., it can be produced as a result of the activity of some enzymes). However, high levels of H₂O₂ have cytotoxic effects.[11,12]

The expensive necessity for highly qualified personnel as well as the relatively low stability of biosensors involved in the use of chromatographic methods of analysis, makes it imperative to develop analytical methods based on stable and comparatively cheap materials that allow for both fast and facile detection of these analytes over a wide range of concentrations.

For this purpose, electrochemical nonenzymatic glucose, fructose and H₂O₂ sensors are a very promising alternative.[13,14] Among the materials employed for the fabrication of these types of devices, gold and platinum nanoparticles[15–17] as well as copper, cobalt or nickel oxides[18,19] have shown the best performance for glucose, fructose and H₂O₂ anodic oxidation in basic aqueous media. Metal and metal oxide micro- and nanostructured particles can be synthesized by many different routes, and although chemical deposition methods have been more studied and developed, electrochemical methods are very promising and have recently attracted much attention due to their versatility. Because of its intrinsic nature and by means of the proper choice of current and/or potential perturbation programs during electrodeposition, this kind of preparation method offers the possibility to carefully control the rate of particle nucleation and growth.[20] In particular, pulse potentiostatic methods have been shown to be useful in controlling the particle size distribution,[21] whereas potential cycling methods lead to more uniform particle growth and composition at the deposit surface.[22] Moreover, the composition of the metallic precursor solution usually affects the electrodeposition process in such a way that particles with different morphologies can be obtained at the surface of the electrode.[20]

Copper is an abundant element in the Earth's crust, and its oxides are not only well known for being stable but also for their multiple electrical and optical properties.[23] Specifically, CuO and Cu₂O can be obtained by using both anodic and cathodic electrodeposition methods. In the first case, a pulse with a sufficiently high potential is applied to produce the oxidation of water or hydroxyl ions at the surface of the electrode, hence attaining a local *pH* decrease, resulting in the precipitation of CuO.[24] On the other hand, in cathodic electrodeposition, a pulse with a sufficiently negative current or low potential is applied to reduce Cu(II) to Cu(I), which precipitates in the form of Cu₂O at the electrode surface.[25] Many studies[26–28] exhibit the versatility of both methods, showing that composition, morphology and particle size are highly influenced by the electrodeposition parameters and conditions, although the relationship between the two and the performance of the fabricated electrodes also depends

on the specific field of application. For example, Siegfried and Choi[29] prepared Cu₂O crystals over an ITO surface by cathodic electrodeposition at different temperatures over the temperature range of 40–70 °C in the absence or presence of 5 wt % SDS, obtaining many variations of cubic and octahedral morphologies over the course of the electrodeposition process. On the other hand, Sasano and others prepared CuO films over Au/Si by single and multiple pulse anodic electrodeposition, obtaining a different crystallinity and photoelectrochemical characteristics in each case.[30]

A mixture of cobalt oxides (abbreviated as CoOx) is a relatively inexpensive and very stable material that shows an efficient catalytic effect over the anodic oxidation of glucose in alkaline media.[31] CoOx deposition can be successfully achieved by electrochemical means in a variety of ways, such as the anodic oxidation of Co(II) soluble tartrate complexes in moderately basic media to obtain Co(III) and Co(IV) oxides.[32] In this work, we propose an interesting alternative that consists of a two-step methodology. Therefore, in the first step, Co is cathodically electrodeposited in a controlled manner over the electrode surface by a single pulse potentiostatic method, while in a second step, the oxidation of metallic Co is realized by a cycling potential method to obtain a uniform film of Co(OH)₂, Co₃O₄, CoOOH, CoO₂ or a mixture of these compounds, depending on the magnitude of the cycled potential interval.[33]

In this work, CuO-, Cu₂O- and CoOx-modified electrodes were prepared by electrodeposition over glassy carbon electrodes (GCEs) by means of pulse potentiostatic methods or by a combination of these methods with potential cycling methods, with the aim of studying the influence of the parameters and conditions of preparation on the performance of the deposited oxides and their morphology. The fabricated electrodes show relatively high sensitivities (i.e., 1929.7 μA mM⁻¹ cm⁻² for glucose and 2923.4 μA mM⁻¹ cm⁻² for fructose with a Cu₂O/GCE) and detection limits on the order of 10⁻⁴ M for glucose, fructose or H₂O₂ in aqueous solutions, even with a simple architecture, compared to other, much more complicated systems.[34] Additionally, some insights into the glucose electrooxidation mechanism over the Cu₂O/GCE- and CoOx/GCE-modified electrodes are also discussed based on the experimental results obtained.

2. EXPERIMENTAL

2.1. Reagents and solutions

Copper(II) nitrate trihydrate (AR, Técnica Química), cobalt(II) nitrate hexahydrate (AR, Mallinckrodt), sodium hydroxide (≥ 98%, Sigma–Aldrich), nitric acid solution (65%, ACS reagent, J.T. Baker), ammonium hydroxide solution (28%, ACS reagent, Sigma–Aldrich), hydrogen peroxide solution (30%, AR, Química Rique), glacial acetic acid (99.9%, J.T. Baker), anhydrous sodium acetate (AR, Monterrey), potassium nitrate (ACS reagent, Química Meyer), D-(+)-glucose (ACS reagent, Sigma–Aldrich), and D-(-)-fructose (99%, Aldrich).

2.2. Apparatus

All electrochemical experiments and measurements were performed with a CHI-920C potentiostat using a typical three-electrode cell employing a Ag/AgCl in 1 M KCl reference electrode (CHI Instruments), a graphite rod as an auxiliary electrode and glassy carbon disk electrodes (CHI Instruments, $d = 3$ mm) as working electrodes. Before each use, the working GCE was consecutively polished with alumina slurries with a particle size of 1, 0.3 and 0.05 μm until a mirror finish was obtained and then finally rinsed with copious amounts of deionized water (18.2 $\text{M}\Omega$ cm) obtained from a PureLab Ultra (Elga) station. pH adjustment of the Cu(II) solutions was achieved by adding proper amounts of 0.1 M NaOH or concentrated ammonium hydroxide solution, while the pH value in the solutions was measured with a Sigma–Aldrich Ag/AgCl pH glass combination electrode and an Orion 5 Star pH -meter (Thermo Scientific). For the case of Co(II), solutions were prepared with the aid of a 0.1 M acetic acid/acetate buffer. SEM characterization of the modified electrodes was carried out with a JEOL JSM-5900 electronic microscope using secondary and backscattered electron imaging. Heating during the electrodeposition experiments at 65 $^{\circ}\text{C}$ was achieved with a conventional hot plate.

2.3. Methodology

For the case of the anodic electrodeposition of CuO, preliminary linear sweep voltammetry experiments at low scan rates (5 mV s^{-1}) were carried out to determine the potential at which water or hydroxyl ions are oxidized in the metallic precursor solution. For this purpose, 0.025 M $\text{Cu}(\text{NO}_3)_2 \cdot 3\text{H}_2\text{O}$ and 0.5 M $\text{NH}_3/\text{NH}_4^+$ at $pH = 8.2$ buffer solutions were used. Subsequently, the single pulse potentiostatic method was applied at different potential pulse magnitudes within the potential interval of 1.050–1.300 V with a pulse duration of 300 s. In this set of experiments, 0.025 M $\text{KNO}_3/0.5 \text{ M NH}_3/\text{NH}_4^+$ solutions were used as blank solutions.

For the cathodic electrodeposition of Cu_2O , a cyclic voltammetry study at two different temperatures (25 and 65 $^{\circ}\text{C}$) in 0.02 M $\text{Cu}(\text{NO}_3)_2 \cdot 3\text{H}_2\text{O}$ at $pH = 4.9$ was carried out first so that an adequate potential interval for Cu(II) electroreduction at each temperature could be found. Afterward, the single pulse potentiostatic method was applied at each temperature with pulses of variable magnitude and a constant duration of 300 s.

CoOx electrodeposition was achieved through a two-step process. In the first step, a cathodic potential pulse was applied for 60 s in the presence of 5 mM $\text{Co}(\text{NO}_3)_2 \cdot 6\text{H}_2\text{O}$ in 0.1 M acetate buffer solution at $pH = 4$. The adequate magnitude for the applied potential was verified by means of a previous study using cyclic voltammetry (100 mV s^{-1}) in the same media. The second step involves the progressive oxidation of the metallic Co particles in a 0.1 M NaOH solution by the application of a cycling potential program in the potential interval of -0.500–0.700 V (30 cycles at 100 mV s^{-1}).

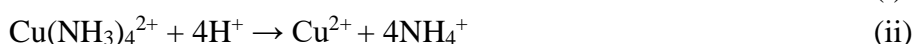
The effect of electrode modification by the electrodeposition procedures was tested by evaluating the corresponding analytical performance of all the prepared modified electrodes in glucose and, in some cases, fructose or H_2O_2 electrooxidation, which was studied by linear sweep voltammetry (LSV) at 100 mV s^{-1} in 0.1 M NaOH media. Some insights into the corresponding electrooxidation mechanisms were collected by a scan rate study using the same technique. Finally, SEM/SEM–EDS analysis of the

modified electrodes was used for the microscopic morphological and chemical characterization of the electrodeposits.

3. RESULTS AND DISCUSSION

3.1. Anodic CuO electrodeposition

According to Izaki and others,[24] anodic electrodeposition of CuO takes place according to the following reactions:



Therefore, if a single potentiostatic pulse can promote reaction i at the surface of the working electrode, CuO formation will be expected to occur as a consequence of the instantaneous corresponding decrease in pH at the Nernst diffusion layer, as indicated by the Pourbaix diagram in Figure SI.1 (see Supporting Information). Figure SI.1 also indicates that this treatment will be more effective if the *pH* value of the Cu(II) solution is as close as possible to 8.1. Experimentally, an adequate potential magnitude for achieving reaction i at the surface of the working electrode was found by linear sweep voltammetry experiments at a low scan rate (5 mV s^{-1}) in 0.025 M Cu(II) solutions and 0.5 M $\text{NH}_3/\text{NH}_4^+$ at *pH* = 8.2 buffered media. For comparison purposes, 0.025 M $\text{KNO}_3/0.5 \text{ M NH}_3/\text{NH}_4^+$ solutions were used as a blank. Figure SI.2 shows the difference in the current-potential responses in the absence and presence of Cu(II). The oxidation signal in figure SI.2A is ascribed to hydroxyl ion oxidation instead of water (reaction v), as was referred by Izaki,[24] since the voltammetric response reaches a plateau, and, hence, it is not the anodic barrier.



As shown in Figure SI.2B, it is clear that the same oxidation signal has a ca. 200 mV lower onset potential. This signal displacement can be explained by the well-known electrocatalytic effect of CuO toward the oxygen evolution reaction (OER).[35] Some current spikes are observed in the voltammogram shown in Figure SI.2B, which can be attributed to the observed accumulation and subsequent release of bubbles of molecular oxygen at the electrode surface. According to these results and aiming to obtain a satisfactory CuO deposit, anodic pulses with a duration of 300 s at $1.050 < E_{app} < 1.300 \text{ V vs. Ag/AgCl}$ from an initial potential, E_0 , of 900 mV vs. Ag/AgCl were applied at the working electrode, as indicated in Table 1. The corresponding current-time responses for the different electrodeposition conditions are shown in Figure 1.

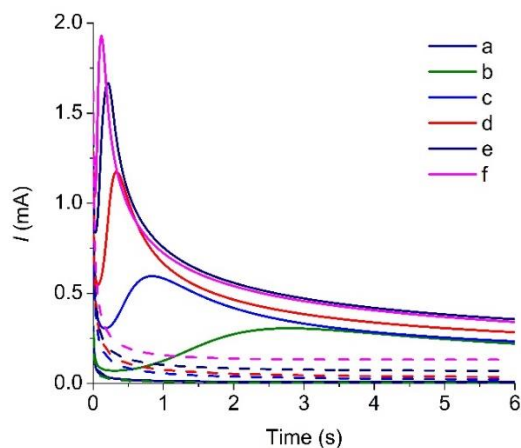


Figure 1. Current-time responses obtained during the anodic electrodeposition treatments listed in Table 1 in the absence (dashed lines) and presence (solid lines) of Cu(II).

The chronoamperometric curves recorded in the presence of Cu(II) present a peak-shaped profile for $t < 5$ s, which is indicative of the formation of a new phase (presumably CuO) at the electrode surface. I vs. t profiles for the same treatments listed in Table 1 but performed with 0.025 M $\text{KNO}_3/0.5$ M $\text{NH}_3/\text{NH}_4^+$ solutions only show a capacitive exponential decay of current vs. time over the same time scale.

Table 1. Anodic electrodeposition parameters used for CuO in the single pulse potentiostatic method. Initial potential $E_0 = 0.900$ V vs. Ag/AgCl.

Treatment	E_{app} (V)	time (s)
a	1.050	300
b	1.100	300
c	1.150	300
d	1.200	300
e	1.250	300
f	1.300	300

As shown in Figure 2, the best analytical performance for glucose oxidation in 0.1 M NaOH media, represented by the magnitude of the oxidation current recorded at 0.500 V by LSV, is achieved with the electrode modified at $E_{app} = 1.200$ V (treatment d in Table 1). Higher potentials drive the oxygen evolution reaction too fast, resulting in a poorer quality of the copper oxide electrodeposit. The inset shown in Figure 2 clearly shows that glucose electrooxidation is not observed at the GCE. These results indicate that the magnitude of the anodic potential pulse applied during the electrodeposition method must be carefully selected in such a way that the hydroxide ion oxidation reaction proceeds at a moderate rate (at electrode potentials close to 1.200 V, but lower than 1.250 V vs. Ag/AgCl), preventing excessive molecular oxygen accumulation at the electrode surface to enable adequate CuO deposition.

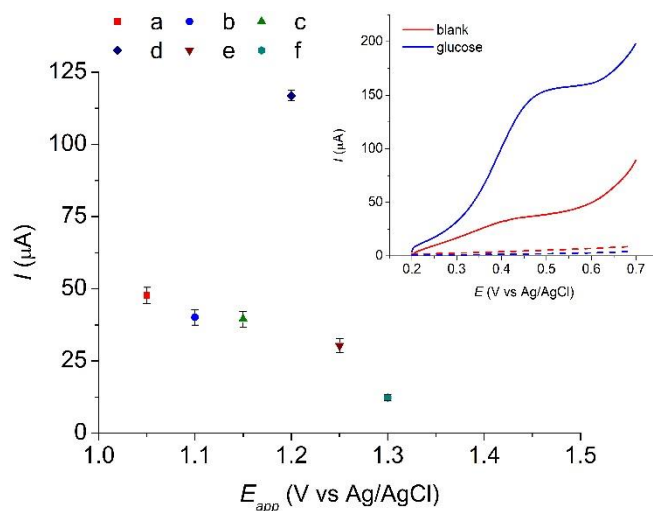


Figure 2. Anodic currents measured (background corrected) for 1 mM glucose electrooxidation at 0.500 V (by LSV recorded at 100 mV s^{-1}) using electrodes modified by the anodic electrodeposition conditions listed in Table 1. Inset: LSV curves in 0.1 M NaOH media in the absence (red) and presence (blue) of 1 mM glucose, recorded with a GCE (dashed lines) and a CuO/GCE (solid lines) fabricated at an E_{app} of 1.200 V. Error bars represent the standard deviation ($n = 3$).

3.2. Cathodic Cu_2O electrodeposition

Electrochemical reduction of dissolved Cu(II) salts in water can yield sparingly soluble Cu(I) oxide under specific conditions. According to Siegfried and others,[29] the corresponding electrochemical reaction of Cu_2O deposition over ITO in slightly acidic media (around $pH = 4.9$) is



As reported by many authors,[36,37] in addition to the reaction temperature and solution pH value, the concentration of complexing and surfactant agents also plays a significant role in the morphology and particle size of the deposited Cu_2O particles. On the one hand, the reaction temperature has an important influence on the electrochemical reaction rate, while on the other hand, the solution composition strongly affects not only the electrical double layer structure but also the mechanism of the deposition reaction. In general, information available in the literature states that control over media temperature, pH and surfactant concentration (such as sodium dodecyl sulfate, SDS) or complexing agents (e.g., lactate or citrate ions) can lead to a mixture of pure cubic and octahedral crystalline behavior.[29,36,37] As a starting point, to carry out a systematic study of the influence of some of these factors on the electrochemical performance of the deposited Cu_2O particles, we calculated the Pourbaix diagram for the Cu(II)/Cu(I)/Cu system at 25°C . The Pourbaix diagram (figure SI.3) shows that the electrochemical reduction of Cu(II) ions to Cu(I) oxide can be achieved in acidic media ($4 < pH < 5$). Experimental validation of this hypothesis was obtained by means of cyclic voltammetry experiments in the presence of $0.02 \text{ M Cu}(\text{NO}_3)_2 \cdot 3\text{H}_2\text{O}$ at $pH = 4.9$, as shown in Figure SI.4A. The potential range at which the desired electrochemical reaction proceeds is approximately $-0.750 < E < -0.400 \text{ V}$, while at $E < -0.750 \text{ V}$, the reduction of Cu(I) to Cu is observed, as can be confirmed by the signal crossover

observed at approximately -1.300 V, which is distinctive evidence of metal electrocrystallization processes.[38]

Based on the previous results, a single potentiostatic pulse with a constant duration of 300 s was applied to induce Cu₂O electrodeposition at either 25 or 65 °C, while varying the applied potential ($-0.800 < E_{app} < -0.500$ V) and looking for the formation of a high amount of dispersed Cu₂O particle nuclei. Figure 3 shows the analytical performance of the prepared Cu₂O-modified electrodes for electrochemical glucose oxidation in 0.1 M NaOH media, represented as the *I* value measured at 0.500 V with LSV. According to these results, electrodes prepared at 25 °C and under an applied potential of -0.600 V for 300 s show the best sensitivity toward glucose oxidation. Notwithstanding that a wider study of the effect of the variables considered in this work on the voltammetric response of Cu₂O-modified glassy carbon electrodes toward glucose oxidation could still be performed, it is possible to establish more appropriate experimental conditions to carry out Cu₂O cathodic electrodeposition and to obtain a maximum sensitivity for glucose electrooxidation.

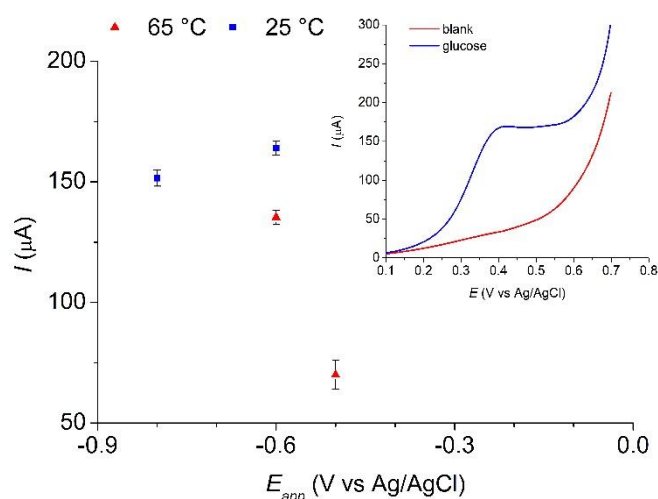
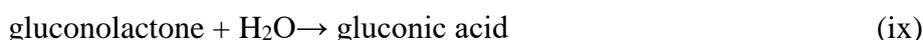
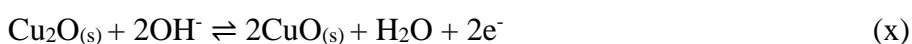


Figure 3. Analytical performance of Cu₂O/GCE prepared by the cathodic electrodeposition method. Inset: LSV curves in 0.1 M NaOH media in the absence (red) and presence (blue) of 1 mM glucose, recorded with the electrodes fabricated at an E_{app} of -0.600 V and 25 °C. Error bars represent the standard deviation ($n = 3$).

The mechanism for glucose electrooxidation on copper(II) oxide in basic aqueous media is usually proposed to consist of the following steps:[39]

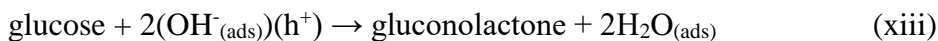


For Cu(I) oxide electrodes, it is assumed that this mechanism is preceded by the following reaction:



However, some authors have recently proposed a different reaction path,[40] arguing that there is not enough evidence for the formation of Cu(III) and establishing that the electrooxidation of glucose

occurs via a two-electron transfer from the carbohydrates to the hydroxyl ions adsorbed on the corresponding copper oxide surface during the anodic scan, followed by the irreversible production of gluconic acid (reaction ix). The driving force for the glucose oxidation reaction (reaction xiii) could then be attributed to the high reactivity of the hydroxyl ion-hole pairs (reaction xi) or of some hydroxyl radicals generated at the electrode surface after the oxidation of adsorbed hydroxyl ions by holes (reaction xii) at the copper oxide surface due to the *p*-type semiconductor properties of this material.



To shed some light on the mechanism of glucose electrooxidation over the Cu₂O/GCE, a scan rate study (10–300 mV s⁻¹) with linear sweep voltammetry was performed in 1 mM glucose and 0.1 M NaOH solutions. Figure SI.5 shows the obtained voltammograms, and Figure 4 indicates the variation in the peak current (measured at 0.500 V vs. Ag/AgCl) and potential (*I_p* and *E_p*) as a function of the scan rate (*v*) on a logarithmic scale. As shown in Figure 4, it is possible to observe that *I_p* is proportional to *v*^{1/2}, indicating that the maximum current for the oxidation signal of glucose depends on the diffusion rate of this species to the electrode and not on the reactivity of a surface-confined species, as would occur if a hypothetical Cu(III) species were involved in the electrochemical process. Figure 4 also shows an anodic displacement for the value of *E_p*, revealing the presence of an irreversible chemical reaction coupled to the glucose oxidation process, in accordance with the qualitative mechanistic diagnostic criteria of Nicholson and Shain.[41]

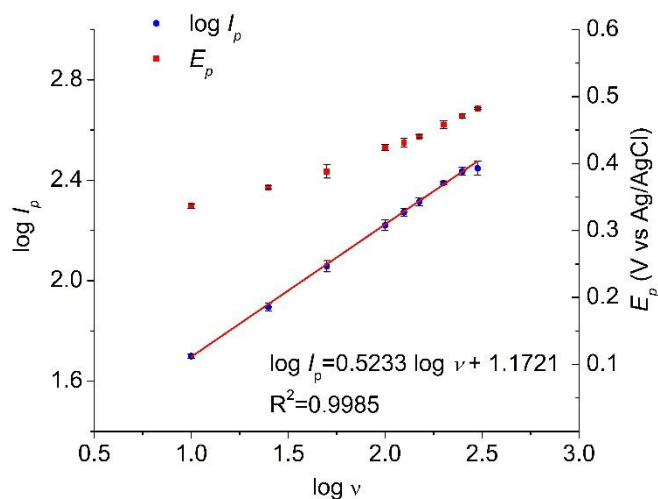


Figure 4. LSV scan rate study (10–300 mV s⁻¹) for the oxidation of 1 mM glucose at Cu₂O/GCE in 0.1 M aqueous NaOH solution. Error bars represent the standard deviation (*n* = 3).

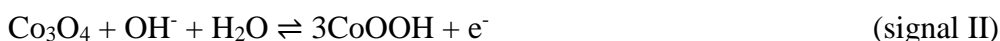
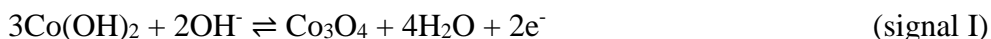
As shown in Figure SI.5, one can also see that the glucose oxidation signal reaches a plateau (a trait that is strongly indicative of a catalytic process), although it could also be attributed to a significant electrode roughness. The LSV curves in the absence of glucose (see figure SI.5) do not reveal any signal

related to the transformation of Cu(I) oxide to any Cu(II) or Cu(III) species within the potential window scanned (0.100–0.700 V vs. Ag/AgCl). Our results suggest that the mechanism proposed by Barragan and others[40] for glucose oxidation over CuO is also valid for Cu₂O-modified electrodes, which is a reasonable assumption since both materials are *p*-type semiconductors.[42,43]

3.3. Two-step CoOx electrodeposition

To determine the optimal conditions for metallic Co deposition on GCE, a cyclic voltammetry study was performed in a 5 mM aqueous Co(NO₃)₂·6H₂O solution with 0.1 M acetate buffer solution (ABS) at *pH* = 4. Figure SI.6A shows the corresponding results of this study, where it is possible to identify the reduction of Co(II) to metallic Co at potentials lower than -0.600 V (signal I_c). The nucleation crossover at approximately -1.200 V is indicative of the aforementioned deposition process, while the oxidation signal with an *E_p* of 0.063 V is associated with the oxidation of the deposited Co to Co(II) (peak I_a). The fabrication of Co/GCE was then achieved by Co electrodeposition on GCE through the application of a potential pulse of -1.200 V for 60 s. Figure SI.6B shows the chronoamperometric profile for the potentiostatic Co deposition process, where three distinctive time zones can be clearly identified: the first zone occurs at very short times (*t* < 0.3 s), with an initial current spike associated with the charge/discharge process of the electrical double layer, followed by a zone in which there is a significant increment (0.3 s < *t* < 3 s) in the current magnitude due to metallic particle nucleation and growth processes, to finally reach a zone with a current decay over time (*t* > 3 s), owing to the diffusive control of the reduction reaction.

The Pourbaix diagram shown in Figure SI.7 reveals that in highly alkaline media (10 < *pH* < 13), metallic Co can be successively oxidized to Co(II) in the form of Co(OH)_{2(s)}, a mixture of Co(II) and Co(III) (Co₃O_{4(s)}), Co(III) as the oxyhydroxide CoOOH_(s) and Co(IV) in the form of the corresponding oxide (CoO_{2(s)}). Adequate control of the electrode/solution interface potential is then essential to obtain a given composition of the oxidized Co particles over the GCE (CoOx/GCE). Co/GCE were then submitted to a potential cycling treatment in 0.1 M NaOH media, applying a total of 30 cycles in the potential range of -0.500 to 0.700 V at 100 mV s⁻¹. Figure SI.8 presents the results of this treatment, where it is possible to identify 3 signals (I-III). According to the Pourbaix diagram shown in Figure SI.7 and as proposed in the related literature,[33,44] these signals are associated with the following electrochemical reactions:



In the first sweep toward positive potential values, an intense and wide oxidation peak is observed, which corresponds to the oxidation of metallic Co to form Co(OH)₂, Co₃O₄ and CoOOH. As the number of cycles increases, there is a significant amount of metallic Co that is converted into Co(II) and Co(III) oxides and oxyhydroxides, which are less conductive species than metallic Co, so a progressive decrease in the current is observed.

Glucose electrooxidation in basic media (0.1 M NaOH solution) at the CoOx/GCE was examined by LSV at $\nu = 100 \text{ mV s}^{-1}$ for different concentrations of glucose in solution. The results obtained are shown in Figure 5, where one can clearly see that the current value for signal III_a increases proportionally with the glucose concentration. Peaks II_a/II_c remain almost unaltered by the glucose concentration and the number of measurements carried out, thus indicating a high stability of the CoOx surface.

It is worth highlighting that, as mentioned before, when the glucose concentration increases, signal III_a increases proportionally, while at the same time, signal III_c decreases proportionally to the glucose concentration. This behavior is a strong indication of the activity of the CoO₂/CoOOH couple as a redox mediator for glucose electrooxidation. To verify this hypothesis, a scan rate study in a 0.91 mM glucose solution was performed. A summary of the obtained results is presented in Figure SI.9, where we can clearly observe how, independent of the scan rate, the current magnitude in the reverse scan is significantly lower in the presence of glucose than in its absence. This effect can be explained by the following proposed catalytic mechanism:

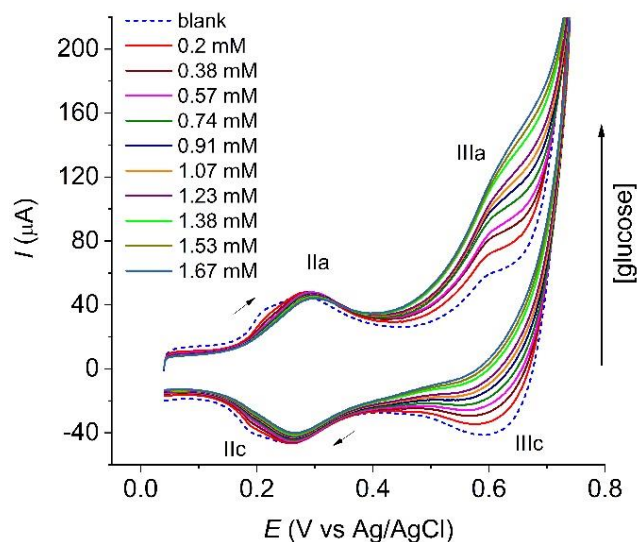
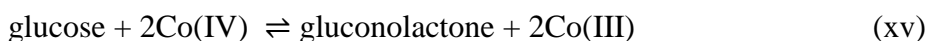


Figure 5. CV curves measured in the absence (dashed line) and presence (solid lines) of glucose at different concentrations (0.2–1.67 mM) in 0.1 M NaOH media. Working electrode: CoOx/GCE. $\nu = 100 \text{ mV s}^{-1}$.

As shown in Figure 6, the current difference between the voltammetric curves measured in the presence and absence of glucose (ΔI) gives a clearer idea of how much higher the measured oxidation currents are in the presence of glucose at the backward scan as a consequence of Co(III) regeneration, when reaction (xv) has more time to proceed, i.e., at lower scan rates. This latter feature of the CoOx/GCE also contributes to its stability as a nonenzymatic electrode for the quantification of glucose.

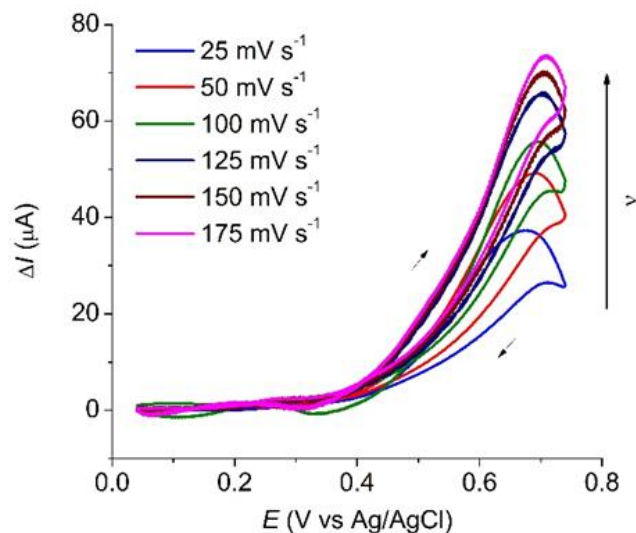


Figure 6. Current difference ($\Delta I = I_{\text{glucose}} - I_{\text{blank}}$) at various scan rates obtained from the CV recorded in the absence or in the presence of 0.91 mM glucose in 0.1 M aqueous NaOH. Working electrode: CoOx/GCE.

3.4. Structural and chemical characterization of the electrode

Figure 7 shows the corresponding SEM images for the Cu₂O/GCE, CuO/GCE and CoOx/GCE electrodes that show the best performance for glucose electrooxidation.

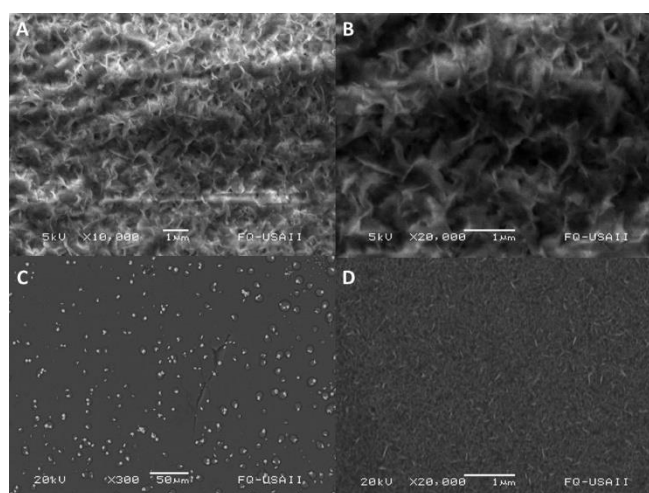


Figure 7. SEM micrographs of Cu₂O/GCE (A and B), CuO/GCE (C) and CoOx/GCE (D) electrodes. Images A, B and D were taken with secondary electrons, while image C was obtained with backscattered electrons.

As shown in Figure 7A, it is possible to observe the electrode surface homogeneously covered by Cu₂O electrodeposited particles with a ridged structure and sizes in the range of less than 1 μm. Figure 7B, at higher magnification, reveals the presence of Cu₂O nanosheets. On the other hand, Figure 7C indicates that electrodeposited CuO particles predominantly form dispersed round particles with diameters in the range of 5-10 μm. Finally, Figure 7D shows the formation of a uniformly distributed electrodeposited CoO_x material at the electrode substrate. Additionally, a rough, needle-like morphology is observed with dimensions on the nanometric scale.

Figures SI.15 – SI.20 show the SEM–EDS results (including elemental mappings and analysis) obtained for the microscopic characterization of the Cu_xO (x = 1,2) and CoO_x electrodeposits. Despite some irregularities observed for the electrodeposits obtained, it is clear that copper, cobalt, and oxygen are present on the corresponding electrode surfaces.

3.5. Analytical application

The analytical performance of the Cu₂O/GC electrodes for glucose, fructose and H₂O₂ quantification was evaluated with linear sweep voltammetry in aqueous 0.1 M NaOH. Figure 8 shows representative LSV curves for individual 1 mM analyte solutions. Additionally, as shown in Figure SI.10, the individual calibration curves with linear relationships between I_p and the concentration of each analyte are contained. The analytical parameters determined from this study are summarized in Table 2. From this table, it can be concluded that glucose, fructose and H₂O₂ can be analyzed by using this technique with limit of detection (LOD) values as low as 55, 86 and 118 μM, respectively, over a wide linear range of concentrations.

Glucose concentrations of approximately 5-7 mM and 3–6 mM are representative of normal levels found in human blood and urine, respectively.[1] The prepared Cu₂O/GCE electrodes are thus excellent candidates for use in glucose content determination in human blood or even in urine. However, from the LSV curves shown in Figure 8, it is clear that both glucose and fructose show oxidation signals that appear at very similar potentials but with different sensitivities. This selectivity problem can be solved by exclusively analyzing the fructose content in real samples by differential pulse polarography in a 1 M CaCl₂ medium.[45] Usually, this latter method is used in addition to the Lane-Eynon titration, which allows for the determination of the total reducing sugar content in complex mixtures. According to the results presented in this section, Cu₂O/GCE can be employed as an alternative to Lane-Eynon titration in the quantification of the total amount of glucose and fructose (e.g., honey samples).

Another alternative for selective sugar determination is the use of the Cu₂O/GCE as a first-generation amperometric glucose sensor,[46] performing in the first place the treatment of the corresponding sample with glucose oxidase, followed by simultaneous quantification without interference from the H₂O₂ produced and the already existing fructose by means of their corresponding oxidation peak currents in LSV.

The response of CuO/GCE and CoO_x/GCE prepared with optimum conditions was also tested in LSV experiments at 100 mV s⁻¹ and different concentrations of glucose in aqueous 0.1 M NaOH solutions. Figures SI.11B and SI.12 show the calibration curves obtained with each electrode, and Table

2 indicates their corresponding analytical parameters. The sensitivity for glucose electrooxidation using the $\text{Cu}_x\text{O}/\text{GCE}$ ($x = 1$ or 2) electrodes is found to be comparable to that reported in a recent related paper.[47]

Table 2. Analytical parameters determined for the different analytes and modified electrodes.

Analyte	Electrode	Sensitivity ($\mu\text{A mM}^{-1} \text{cm}^{-2}$)	LOD (μM)	R^2
Glucose	CuO/GCE	1414.7	146	0.994
Glucose	$\text{Cu}_2\text{O}/\text{GCE}$	1929.7	55	0.997
Glucose	CoO_x/GCE	621.2	163	0.991
Fructose	$\text{Cu}_2\text{O}/\text{GCE}$	2923.4	86	0.994
H_2O_2	$\text{Cu}_2\text{O}/\text{GCE}$	455.6	118	0.998

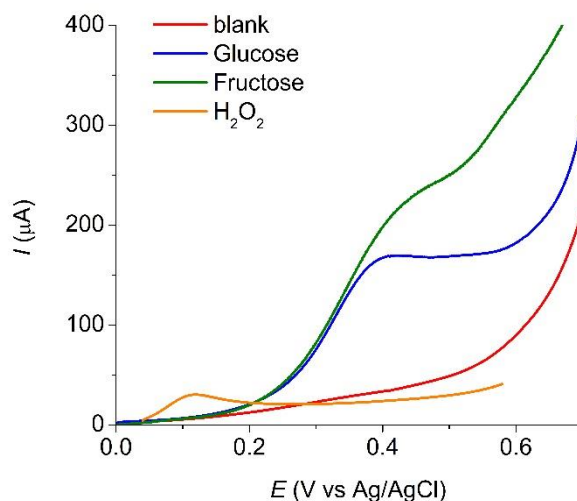


Figure 8. Typical LSV curves ($v = 100 \text{ mV s}^{-1}$) for individual 1 mM solutions of glucose, fructose or H_2O_2 in 0.1 M aqueous NaOH. Working electrode: $\text{Cu}_2\text{O}/\text{GCE}$.

In clinical medicine, aqueous glucose solutions (5% w/v) are commonly used intravenously for the treatment and prevention of hypoglycemia and dehydration.[48] As shown in Table 3, we report the results for the analysis of the glucose content of a pharmaceutical formulation (DX-5 commercial solution). For comparison purposes, the same analysis was carried out for a synthetic sample prepared at the same nominal concentration. The analysis was accomplished by using the $\text{Cu}_2\text{O}/\text{GCE}$ electrode with the LSV technique and by measurement of the density of the corresponding sample solutions. The results given in Table 3 indicate that both methods show very similar results, with acceptable statistical

deviations. Hence, the glucose content for both the pharmaceutical and the synthetic samples is found to be close to the nominal value.

Table 3. Analysis results for aqueous glucose solutions.

Sample	Glucose content (% w/v \pm S.D.)		
	Nominal	Measured by	
		Nonenzymatic sensor ^[a]	Density method ^[b]
Pharmaceutical formulation	5.0	5.2 \pm 0.5	4.5 \pm 0.4
Synthetic	5.0	4.6 \pm 0.2	5.0 \pm 0.1

[a] Performed by the standard addition method using LSV and a Cu₂O/GCE working electrode, n = 5 (see. Figures SI.13 and 14). [b] Mass measurement of a known volume of the corresponding solution at 20 °C, n = 3 (see. Table SI.1).

4. CONCLUSION

Cu_xO/GCE (x = 1,2) and CoO_x/GCE electrodes were successfully prepared by potentiostatic or a combination of potentiostatic and potentiodynamic techniques, demonstrating the versatility of these electrochemical methods for the electrodeposition of microstructured metal oxides. Thermodynamic data and voltammetric studies were used to choose appropriate conditions for the electrodeposition experiments. For each system, adequate selection of the electrodeposition parameters and conditions is critical since it greatly influences the analytical performance of the modified electrodes prepared for the electrooxidation of glucose in basic media. The results obtained also indicate that the Cu₂O/GCE electrodes are excellent candidates for the rapid and facile analysis of glucose, fructose and H₂O₂ in real samples with analyte contents on the order of 10⁻⁵ M or higher. We propose that glucose electrooxidation at Cu₂O/GCE electrodes follows an EC mechanism without the participation of Cu(III) species, while this process is mediated via the CoO₂/CoOOH redox couple at the CoO_x/GCE electrodes. The glucose content in pharmaceutical and synthetic aqueous glucose solutions was analyzed by using two different methods, indicating that the Cu₂O/GCE electrode can give reliable and satisfactory results for these samples.

SUPPORTING INFORMATION:

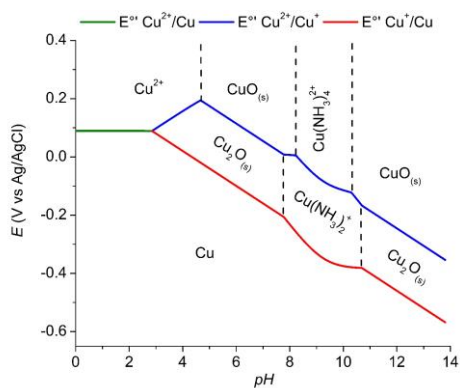


Figure SI.1. E vs. pH diagram for the Cu(II)/Cu(I)/Cu system at a total Cu concentration of 0.025 M in 0.5 M $\text{NH}_3/\text{NH}_4^+$ buffered media at 25 °C. Data used for diagram construction were taken from [49,50].

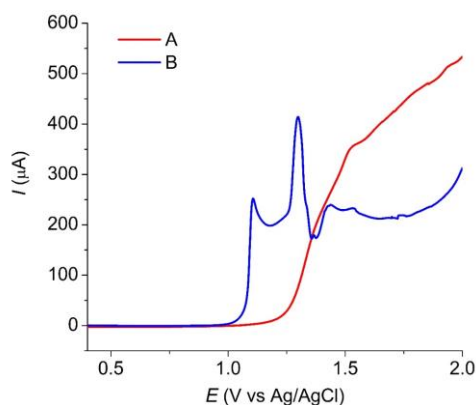


Figure SI.2. LSV curves at 5 mV s^{-1} for (A) 0.025 M KNO_3 and 0.5 M $\text{NH}_3/\text{NH}_4^+$, (B) 0.025 M $\text{Cu}(\text{NO}_3)_2 \cdot 3\text{H}_2\text{O}$ and 0.5 M $\text{NH}_3/\text{NH}_4^+$ at $pH = 8.15$ solutions. Working electrode: glassy carbon disk, with a diameter of 3 mm.

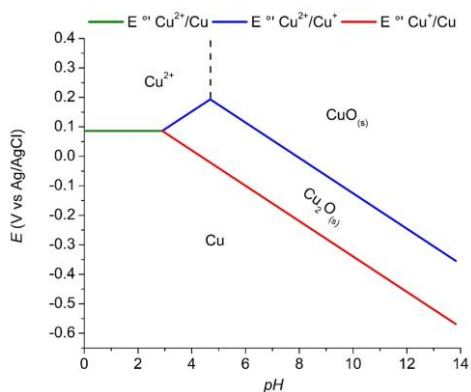


Figure SI.3. E vs. pH diagram for the Cu(II)/Cu(I)/Cu system with a total Cu concentration of 0.02 M at 25 °C. Data used for diagram construction were taken from [49,50].

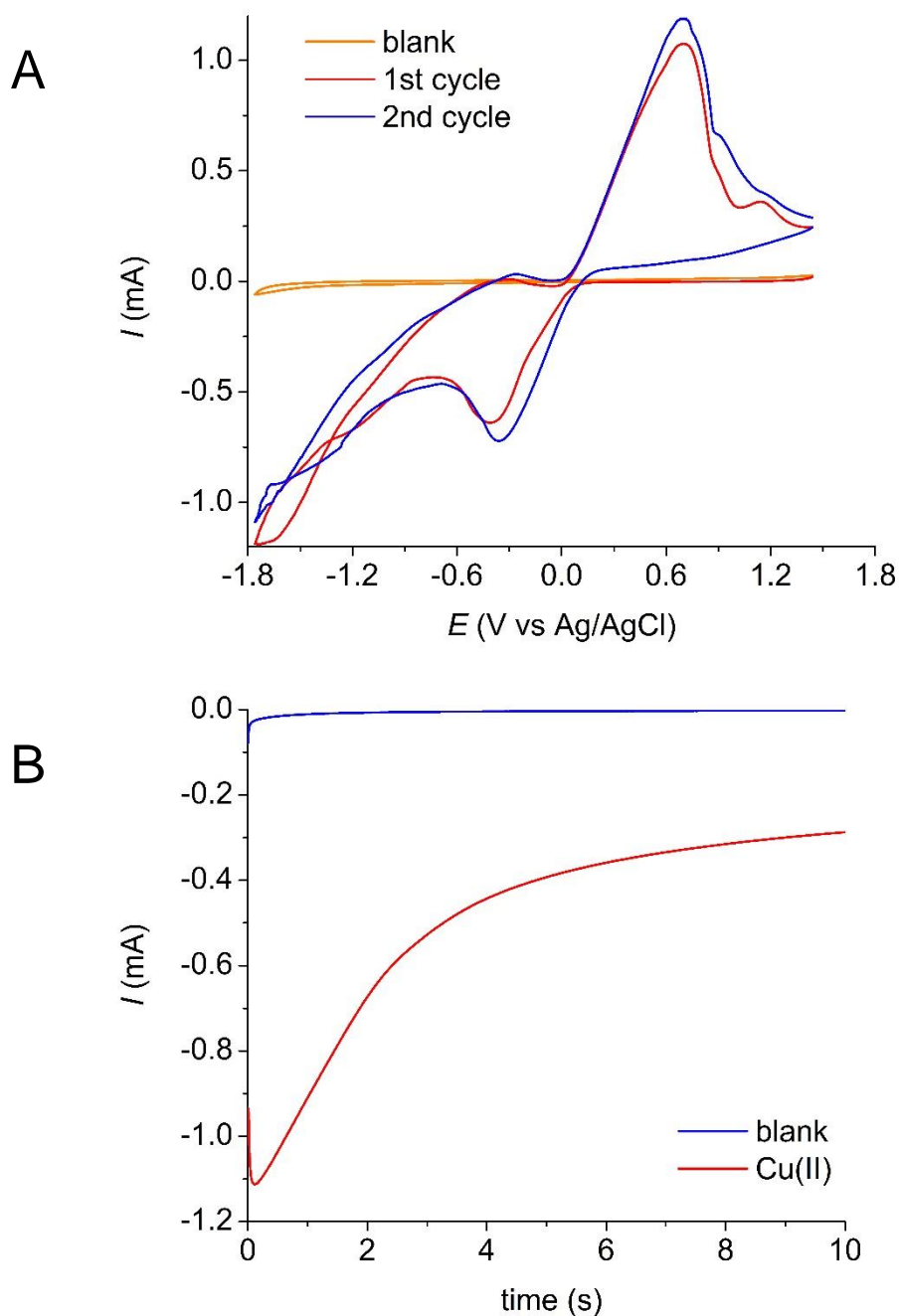


Figure SI.4. A) Cyclic voltammograms measured at 25 °C for 0.02 M $\text{Cu}(\text{NO}_3)_2 \cdot 3\text{H}_2\text{O}$ aqueous solution at $pH = 4.9$. A 0.02 M KNO_3 solution at the same pH was used as a blank. $\nu = 100 \text{ mV s}^{-1}$. B) Chronoamperometric experiments (initial potential $E_0 = 0.300 \text{ V}$, step potential $E_{app} = -0.600 \text{ V}$ vs. Ag/AgCl) in a 0.02 M KNO_3 aqueous solution at $pH = 4.9$ (blank) and in a 0.02 M $\text{Cu}(\text{NO}_3)_2 \cdot 3\text{H}_2\text{O}$ aqueous solution at the same pH . Working electrode: glassy carbon disk, with a diameter of 3 mm.

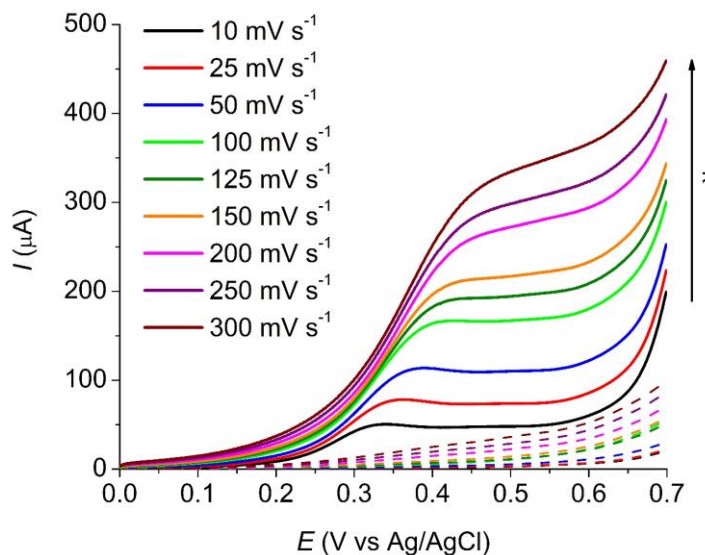


Figure SI.5. LSV curves measured at different scan rates ($10\text{--}300\text{ mV s}^{-1}$) in the absence (dashed lines) and presence (solid lines) of 1 mM glucose in 0.1 M NaOH solutions. Working electrode: $\text{Cu}_2\text{O}/\text{GCE}$ prepared at $25\text{ }^\circ\text{C}$ and $E_{app} = -0.600\text{ V}$ for 300 s .

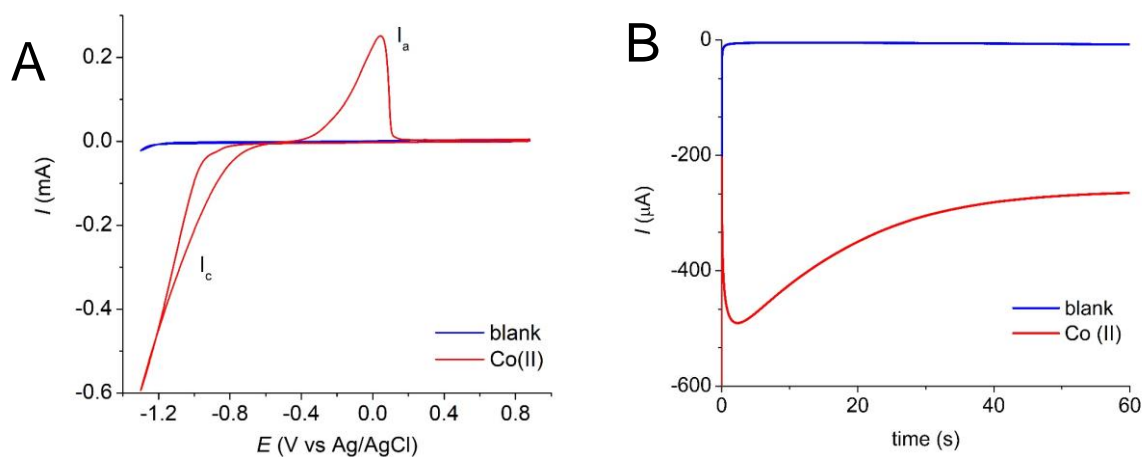


Figure SI.6. A) Cyclic voltammograms measured at 100 mV s^{-1} and $25\text{ }^\circ\text{C}$ for 5 mM $\text{Co}(\text{NO}_3)_2 \cdot 6\text{H}_2\text{O}$ solution at $\text{pH} = 4.0$ in 0.1 M ABS. B) I vs. t profile during the cathodic electrodeposition of Co (initial potential -0.200 V , $E_{app} = -1.200\text{ V}$ vs. Ag/AgCl). Working electrode: glassy carbon disk, with a diameter of 3 mm .

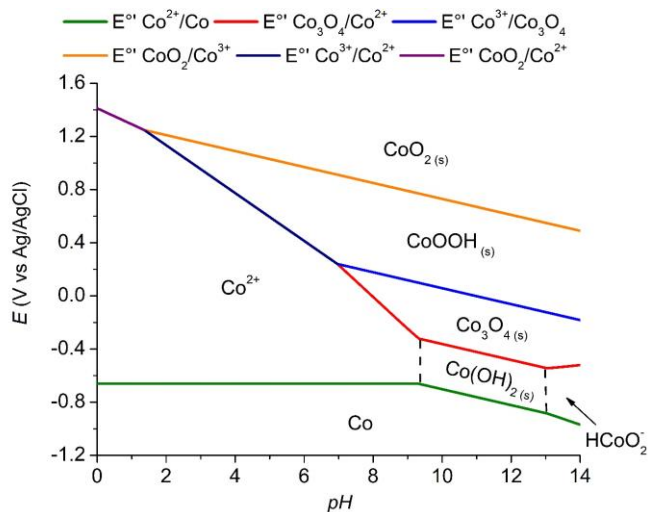


Figure SI.7. E vs. pH diagram for the Co(IV)/Co(III)/Co(II)/Co system at 25 °C and a total Co concentration of 1×10^{-6} M. Data used for diagram construction were taken from [51–53].

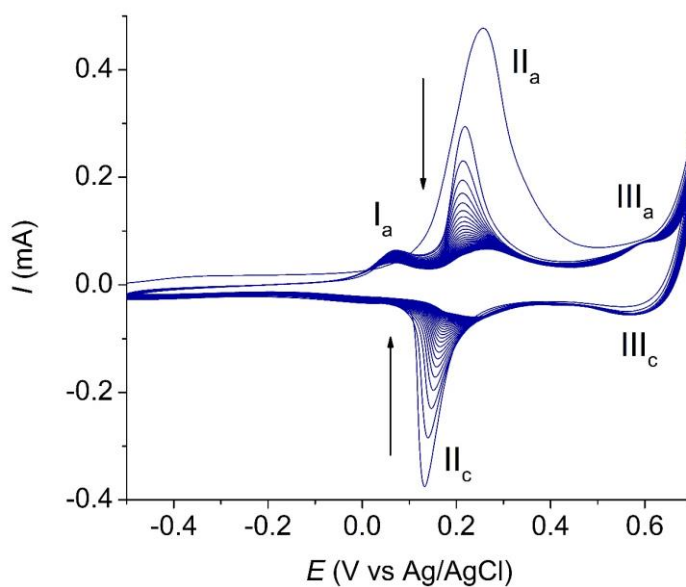


Figure SI.8. Potential cycling treatment for the Co/GCE in 0.1 M NaOH media; 30 cycles at 100 mV s^{-1} .

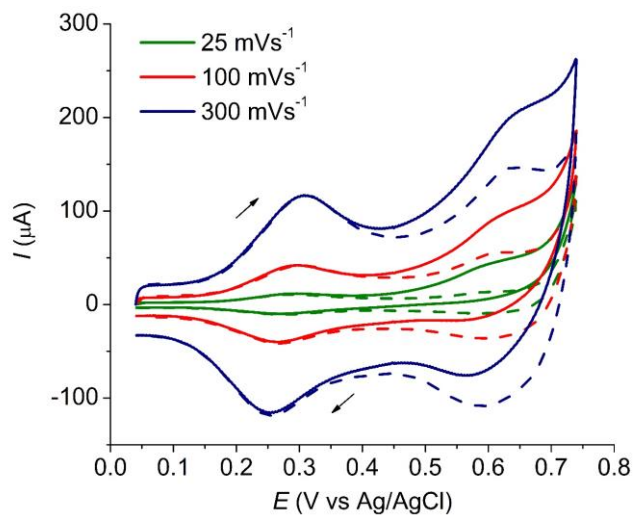


Figure SI.9. Representative cyclic voltammetry curves obtained at different scan rates (25–300 mV s^{-1}) for 0.1 M NaOH media in the absence (dashed lines) and presence (solid lines) of 0.91 mM glucose. Working electrode: CoOx/GCE.

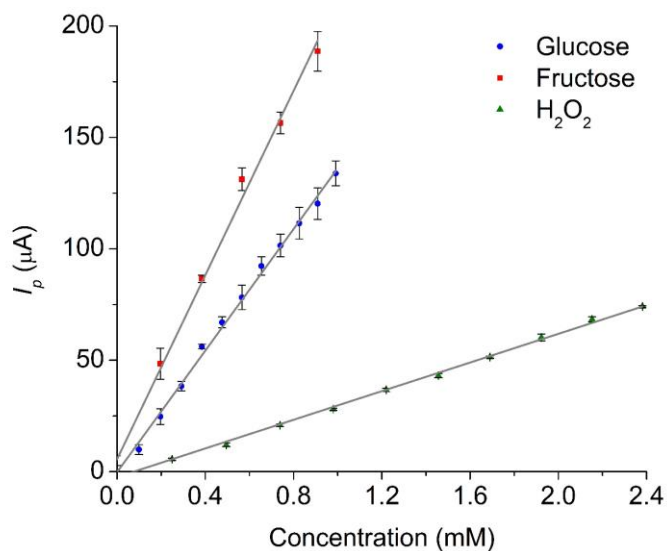


Figure SI.10. Linear scan voltammetry calibration curves for glucose, fructose, and H_2O_2 in 0.1 M NaOH, recorded at 100 mV s^{-1} . Working electrode: $\text{Cu}_2\text{O}/\text{GCE}$. Error bars represent the standard deviation calculated for each data point ($n = 3$).

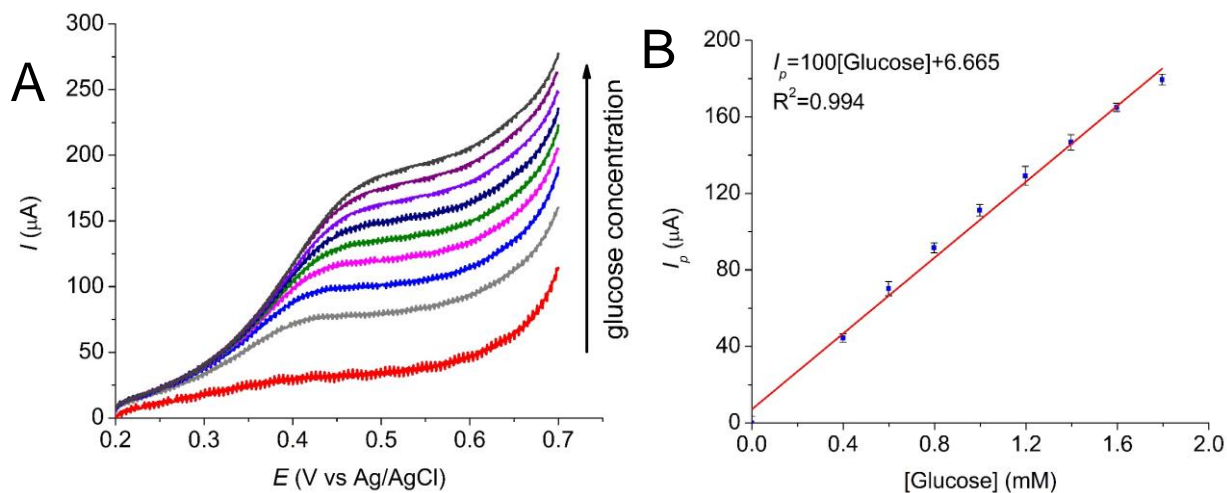


Figure SI.11. A) Linear scan voltammetry curves measured at 100 mV s^{-1} in 0.1 M NaOH media (blank: red line) and different glucose concentrations (0.4 – 1.8 mM). B) Associated calibration curve. Working electrode: CuO/GCE prepared at $E_{app} = 1.200 \text{ V}$ for 300 s . Error bars represent the standard deviation calculated for each data point ($n = 3$).

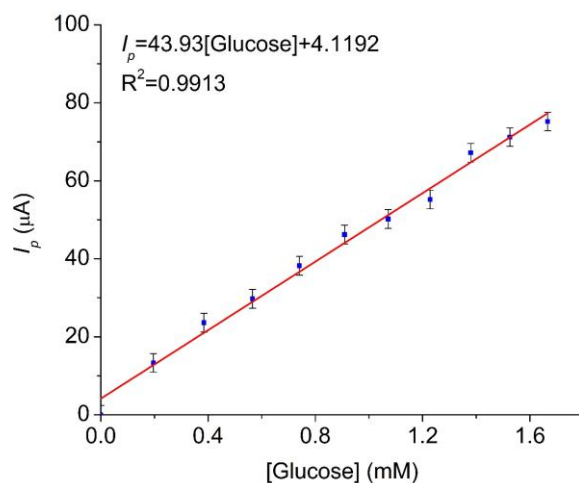


Figure SI.12. Glucose calibration curve. Data obtained from signal III_a in the CV curves recorded in 0.1 M NaOH media. Working electrode: CoOx/GC . $\nu = 100 \text{ mV s}^{-1}$. Error bars represent the standard deviation calculated for each data point ($n = 3$).

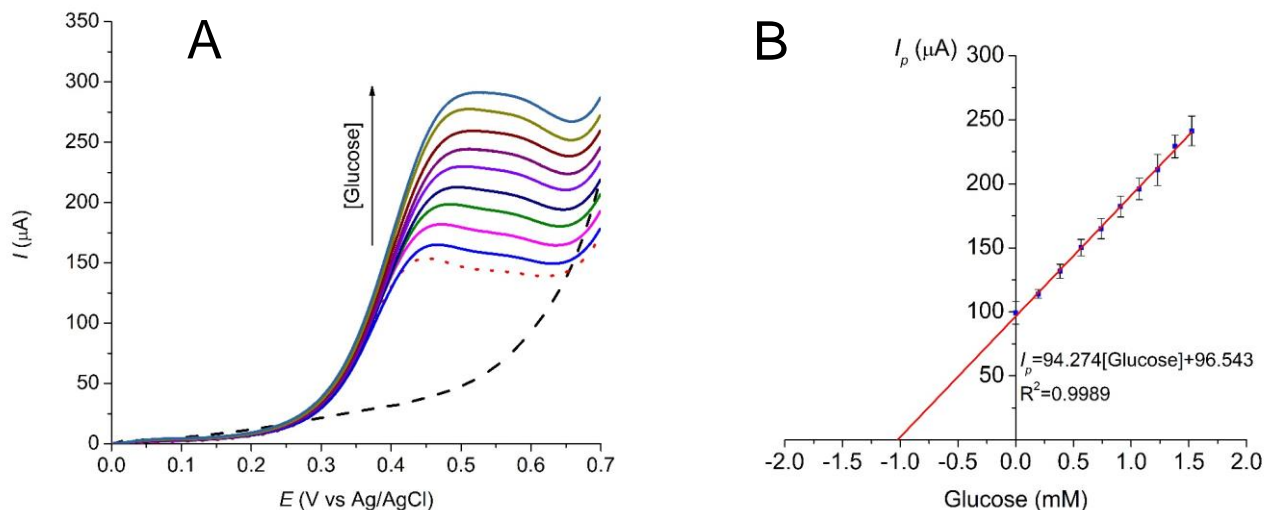


Figure SI.13. A) Representative LSV recorded for addition of a glucose standard to a commercial solution (DX-5) diluted in 0.1 M NaOH media ($v = 100 \text{ mV s}^{-1}$); blank, diluted sample and standard additions are represented by dashed, dotted and solid lines, respectively. B) Associated calibration curve. Working electrode: $\text{Cu}_2\text{O}/\text{GCE}$. Error bars represent the standard deviation calculated for each data point ($n = 3$).

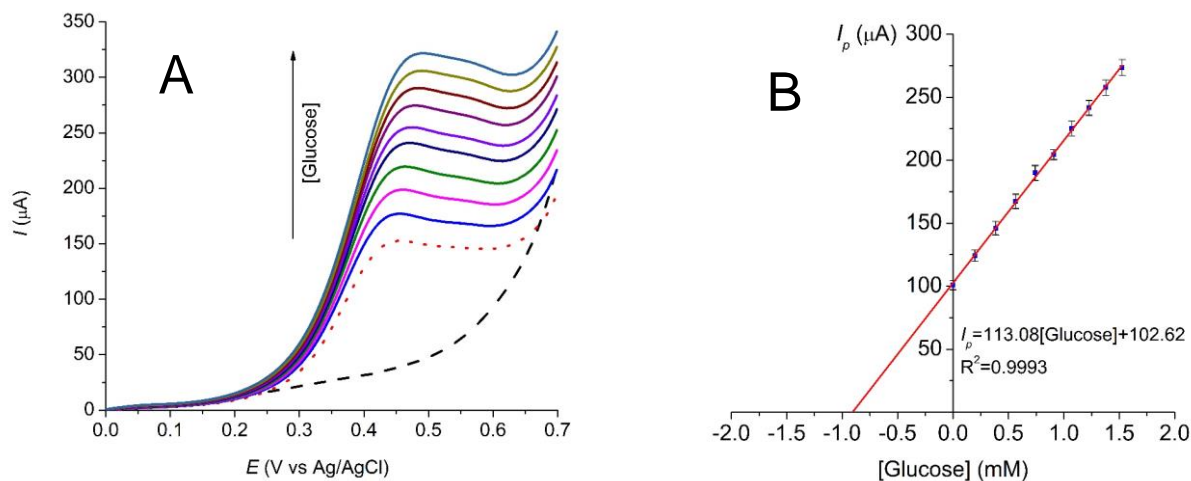


Figure SI.14. A) Representative LSV recorded for the addition of a glucose standard to a synthetic sample diluted in 0.1 M NaOH media ($v = 100 \text{ mV s}^{-1}$); blank, diluted sample and standard added solutions are represented by dashed, dotted and solid lines, respectively. B) Associated calibration curve. Working electrode: $\text{Cu}_2\text{O}/\text{GCE}$. Error bars represent the standard deviation calculated for each data point ($n = 3$).

Table SI.1. Density determination for the aqueous glucose solutions at 20 °C.

Sample	Volume (mL)	Mass (g)	Density (g/mL)	Glucose content (% w/v) [a]
Pharmaceutical	1.0	1.01721	1.01721	5.0
Pharmaceutical	2.0	2.02976	1.01488	4.4
Pharmaceutical	3.0	3.04335	1.01445	4.2
Synthetic	1.0	1.01736	1.01736	5.0
Synthetic	2.0	2.03450	1.01725	5.0
Synthetic	3.0	3.05098	1.01699	4.9

[a] Values estimated using a calibration curve created with values taken from the concentration vs. density table (20 °C).[54]

SEM/SEM-EDS elemental analysis of Cu_xO (x=1,2)-modified or CoO_x-modified glassy carbon electrodes:

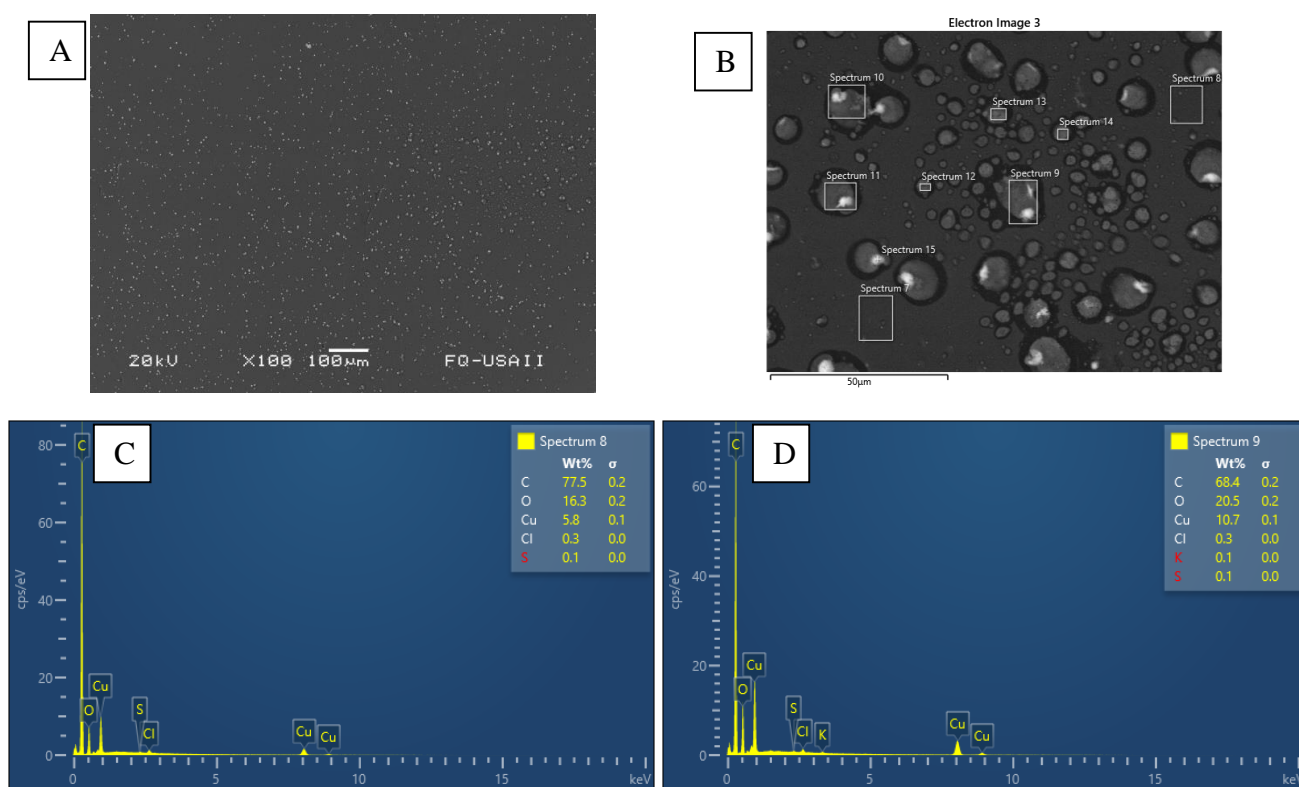


Figure SI.15. Typical EDS spectra measured for CuO/GCE prepared potentiostatically by anodic electrodeposition at $E_{app} = 1.20$ V vs. Ag/AgCl (treatment d in Table 1) in a 0.025 M Cu(NO₃)₂·3H₂O/0.5 M NH₃/NH₄⁺ solution at pH = 8.15. Initial potential $E_0 = 0.900$ V vs. Ag/AgCl. A) SEM image of backscattered electrons (BSE). B) Higher magnification of image A with some areas selected for EDS analysis. C, D) EDS analysis of Spectrum 8 and Spectrum 9 areas in image B.

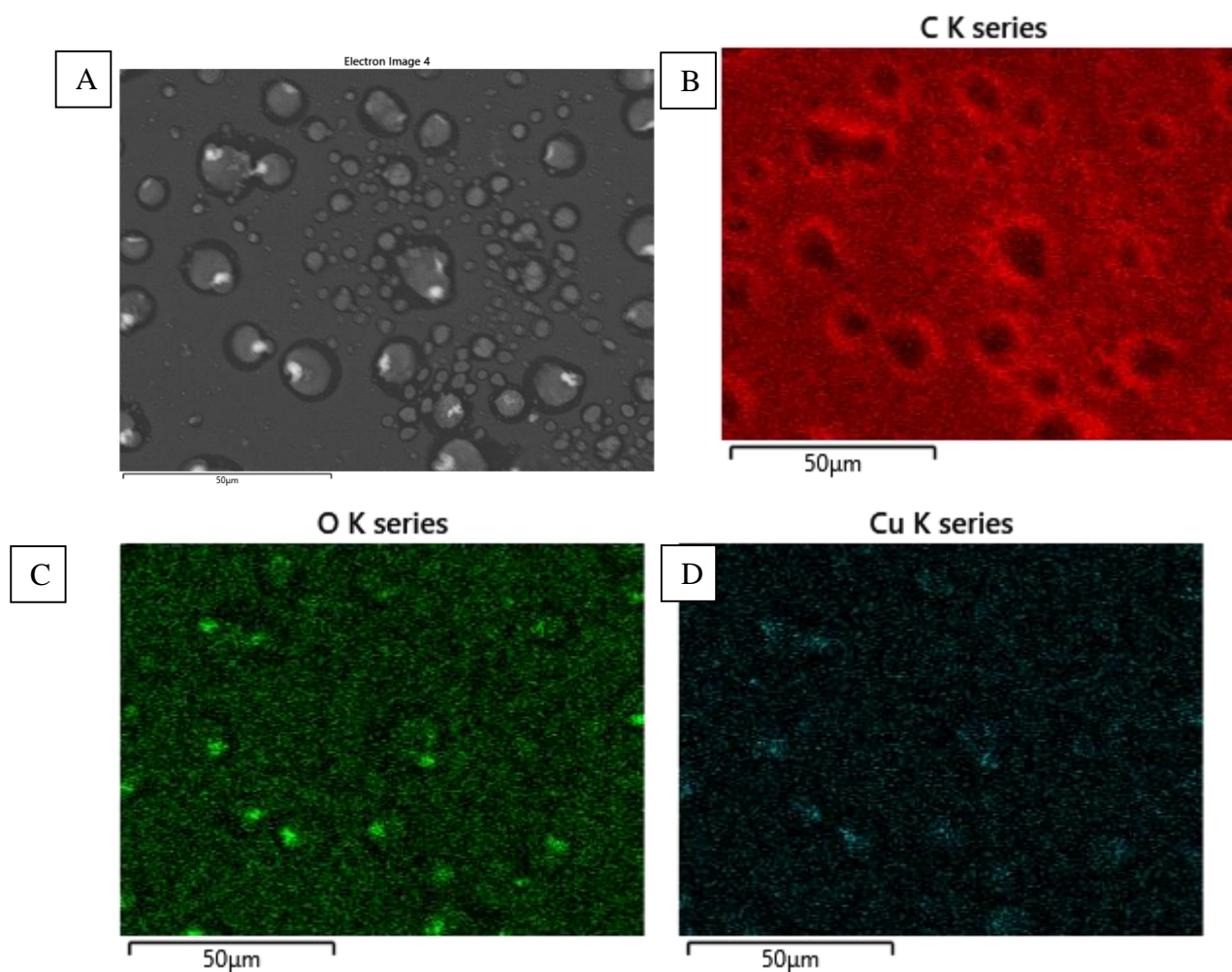


Figure SI.16. SEM image and EDS elemental mapping for CuO/GCE prepared potentiostatically by anodic electrodeposition at $E_{app} = 1.200$ V vs. Ag/AgCl (treatment d in Table 1) in a 0.025 M $\text{Cu}(\text{NO}_3)_2 \cdot 3\text{H}_2\text{O}$ /0.5 M $\text{NH}_3/\text{NH}_4^+$ solution at $pH = 8.15$. Initial potential $E_0 = 0.900$ V vs. Ag/AgCl. A) BSE SEM image. B) C mapping. C) O mapping. D) Cu mapping.

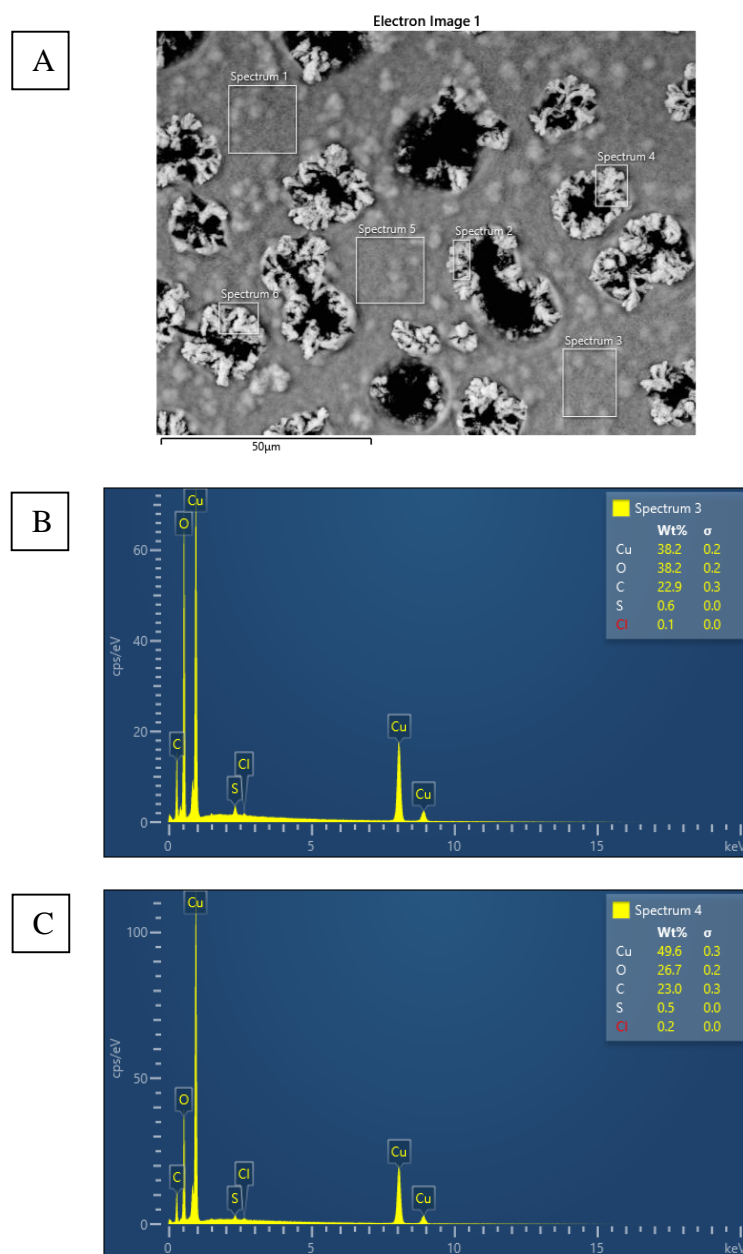


Figure SI.17. SEM image and typical EDS spectra obtained for $\text{Cu}_2\text{O}/\text{GCE}$ prepared potentiostatically by cathodic electrodeposition at $E_{app} = -0.600$ V vs. Ag/AgCl for 300 s in a 0.02 M $\text{Cu}(\text{NO}_3)_2 \cdot 3\text{H}_2\text{O}$ aqueous solution at $\text{pH} = 4.9$. Initial potential $E_0 = 0.300$ V vs. Ag/AgCl. A) BSE SEM image. B) and C) EDS elemental analysis of Spectrum 3 and Spectrum 4 zones in image A.

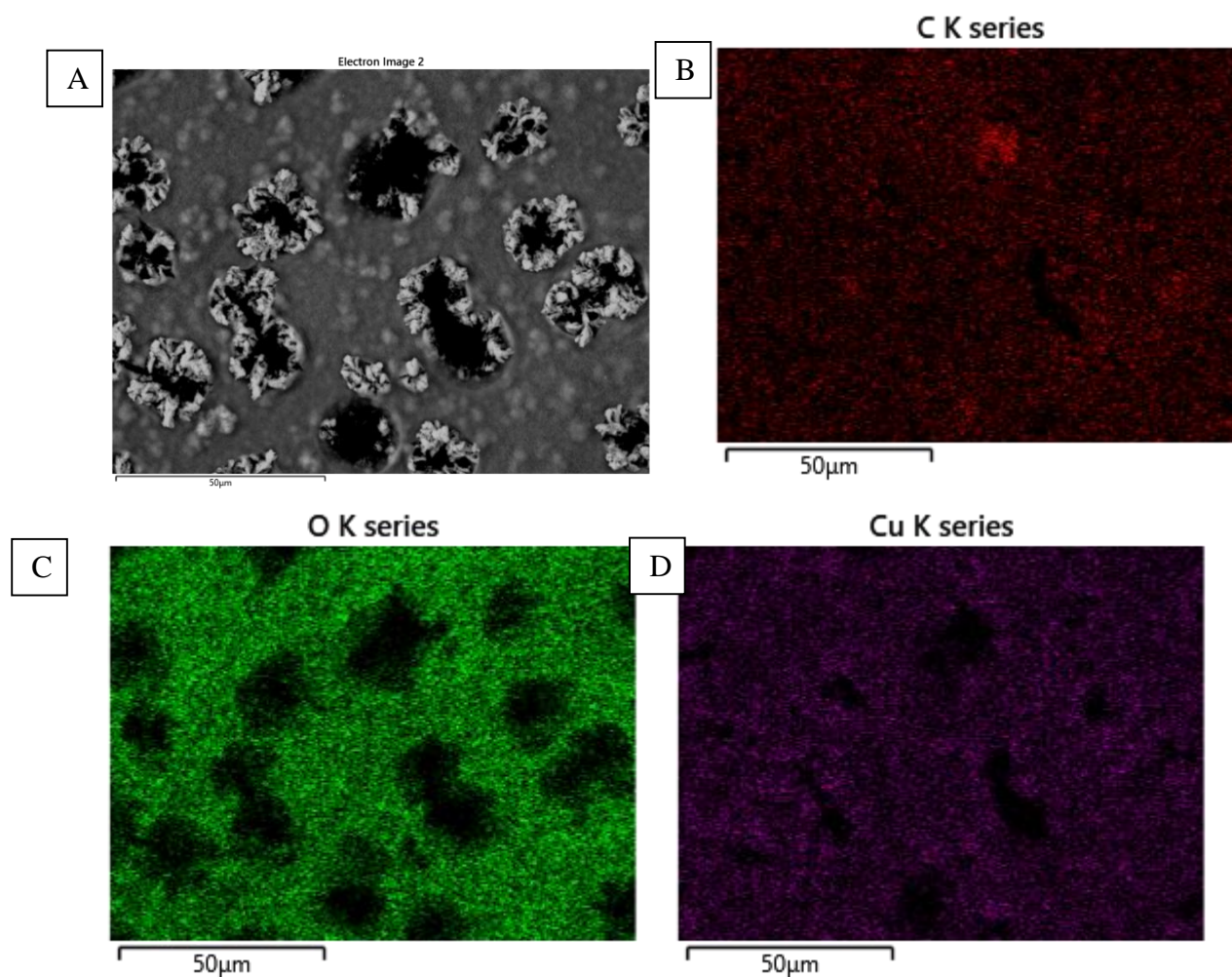


Figure SI.18. SEM and EDS elemental mapping for Cu₂O/GCE prepared potentiostatically by cathodic electrodeposition at $E_{app} = -0.600$ V vs. Ag/AgCl for 300 s in a 0.02 M Cu(NO₃)₂·3H₂O aqueous solution at $pH = 4.9$. Initial potential $E_0 = 0.300$ V vs. Ag/AgCl. A) BSE SEM image. B) C mapping. C) O mapping. D) Cu mapping.

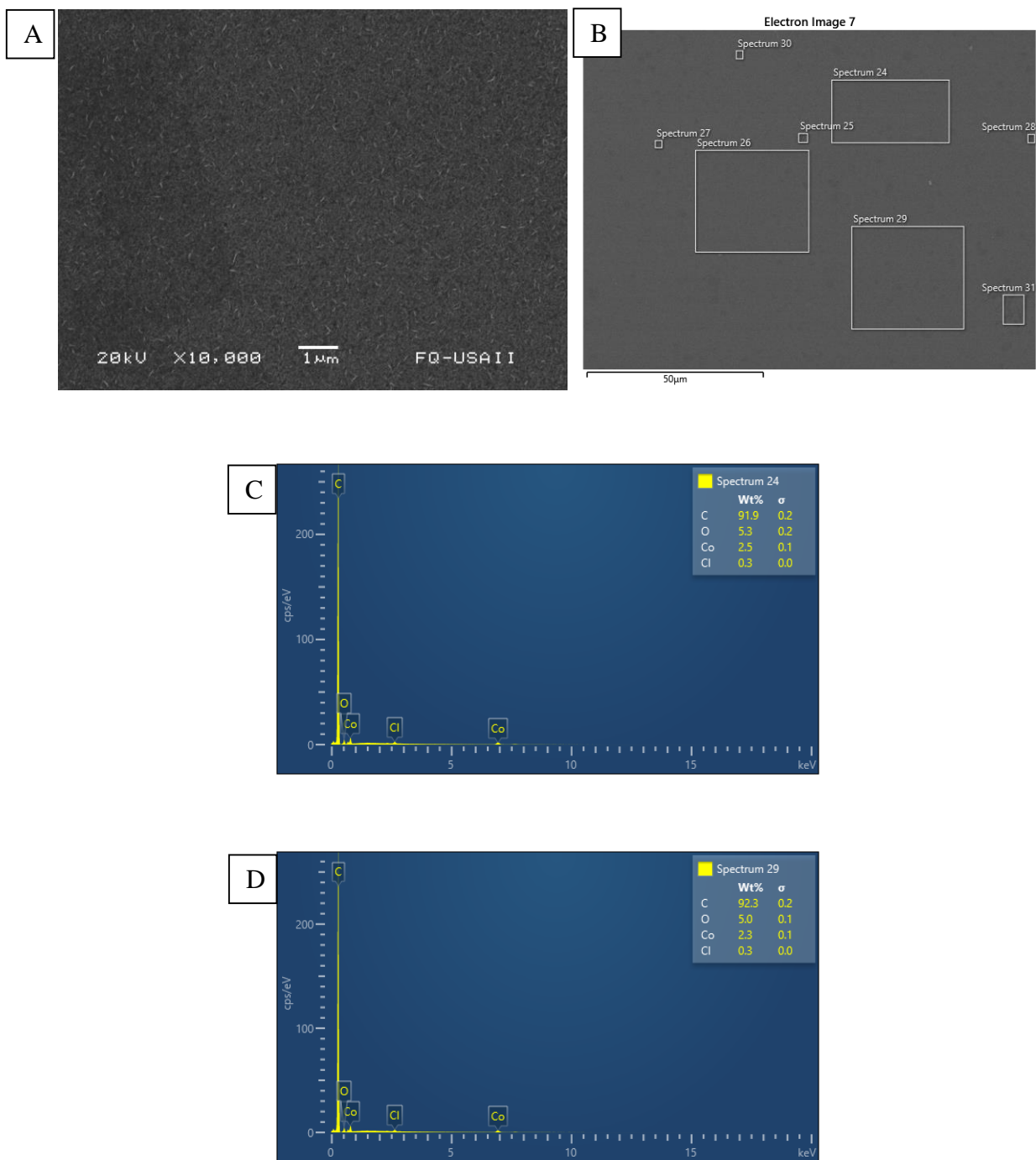


Figure SI.19. SEM images and typical EDS spectra obtained for CoOx/GCE prepared by cobalt deposition at $E_{app} = -1.200$ V vs. Ag/AgCl (cathodic pulse applied for 60 s) in 5 mM $\text{Co}(\text{NO}_3)_2 \cdot 6\text{H}_2\text{O}$ in 0.1 M acetate buffer solution at pH = 4 (first step) followed by progressive oxidation of the metallic Co deposit in a 0.1 M NaOH solution due to the application of a cycling potential program in the interval of -0.500-0.700 V vs. Ag/AgCl (30 cycles at 100 mV s^{-1}). A) and B) SEM images of secondary electrons at different magnifications. C) and D) EDS elemental analysis of Spectrum 24 and Spectrum 29 zones in image B.

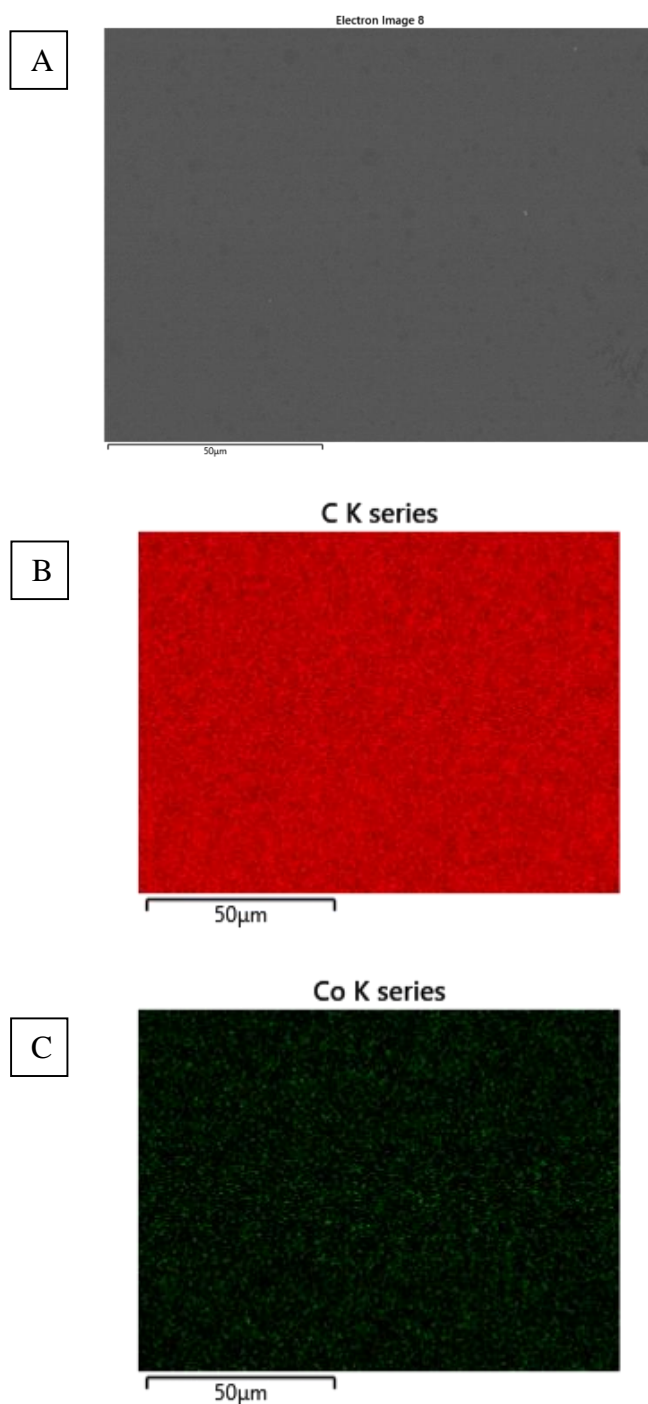


Figure SI.20. EDS elemental mapping of CoOx/GCE prepared by cobalt deposition at $E_{app} = -1.200$ V vs. Ag/AgCl (cathodic pulse applied for 60 s) in 5 mM $\text{Co}(\text{NO}_3)_2 \cdot 6\text{H}_2\text{O}$ in 0.1 M acetate buffer solution at pH = 4 (first step) followed by progressive oxidation of the metallic Co deposit in a 0.1 M NaOH solution due to the application of a potential cycling program in the potential interval of -0.500-0.700 V vs. Ag/AgCl (30 cycles at 100 mV s^{-1}). A) SEM image of secondary electrons. B) C mapping. C) Co mapping.

ACKNOWLEDGMENTS

Ulrich Briones-Guerash S. thanks CONACYT for a Ph. D. scholarship (No. 335875). Julio C. Aguilar-Cordero acknowledges financial support from DGAPA-UNAM (PAPIIT Projects No. 221918 and 222921) and PAIP-FQUNAM (5000-9031). Authors are also in debt to Rafael Iván Puente Lee for his valuable support with the SEM characterization.

References

1. D. Bruen, C. Delaney, L. Florea, D. Diamond, *Sensors*, 17 (2017) 1866.
2. J.C.Y. Louie, H. Moshtaghian, S. Boylan, V.M. Flood, A.M. Rangan, A.W. Barclay, J.C. Brand-Miller, T.P. Gill, *Eur. J. Clin. Nutr.*, 69 (2015) 154.
3. N.S. Oliver, C. Toumazou, A.E.G. Cass, D.G. Johnston, *Diabet. Med.*, 26 (2009) 197.
4. N.M. Al-Mhanna, H. Huebner, R. Buchholz, *Foods*, 7 (2018) 185.
5. S. Ouchemoukh, P. Schweitzer, M. Bachir Bey, H. Djoudad-Kadji, H. Louaileche, *Food Chem.*, 121 (2010) 561.
6. L.C.A. da Silva, J.A.Q. Lafeté Junior, M.O. Leite, E.A.F. Fontes, J.S.R. Coimbra, *Int. J. Dairy Technol.*, 73 (2020) 795.
7. P.W. Alexander, R.D. Hartati, J. Curtin, *Electroanalysis*, 1 (1989) 263.
8. J.N. BeMiller, S.S. Nielsen (Ed.), *Food Analysis*, 4th ed., Springer US, (2010) Boston, MA, pp. 147–177.
9. C. Chen, Q. Xie, D. Yang, H. Xiao, Y. Fu, Y. Tan, S. Yao, *RSC Adv.*, 3 (2013) 4473.
10. I.L. Jernelv, K. Milenko, S.S. Fuglerud, D.R. Hjelm, R. Ellingsen, A. Aksnes, *Appl. Spectrosc. Rev.*, 54 (2019) 543.
11. W. Chen, S. Cai, Q.Q. Ren, W. Wen, Y. Di Zhao, *Analyst*, 137 (2012) 49.
12. J. Meier, E. Hofferber, J.A. Stapleton, N.M. Iverson, *Chemosensors*, 7 (2019) 64.
13. D.W. Hwang, S. Lee, M. Seo, T.D. Chung, *Anal. Chim. Acta*, 1033 (2018) 1.
14. K. Dhara, D.R. Mahapatra, *J. Mater. Sci.*, 54 (2019) 12319.
15. D. Thatikayala, D. Ponnamma, K.K. Sadasivuni, J.J. Cabibihan, A.K. Al-Ali, R.A. Malik, B. Min, *Biosensors*, 10 (2020) 151.
16. P. Si, Y. Huang, T. Wang, J. Ma, *RSC Adv.*, 3 (2013) 3487.
17. S. Chen, R. Yuan, Y. Chai, F. Hu, *Microchim. Acta*, 180 (2013) 15.
18. H. Zhu, L. Li, W. Zhou, Z. Shao, X. Chen, *J. Mater. Chem. B*, 4 (2016) 7333.
19. M.M. Rahman, A.J.S. Ahammad, J.H. Jin, S.J. Ahn, J.J. Lee, *Sensors*, 10 (2010) 4855.
20. B.J. Plowman, S.K. Bhargava, A.P. O'Mullane, *Analyst*, 136 (2011) 5107.
21. M. Ueda, H. Dietz, A. Anders, H. Knepe, A. Meixner, W. Plieth, *Electrochim. Acta*, 48 (2002) 377.
22. E. Kim, N. Kang, J.J. Moon, M. Choi, *Bull. Korean Chem. Soc.*, 37 (2016) 1445.
23. A.S. Zoolfakar, R.A. Rani, A.J. Morfa, A.P. O'Mullane, K. Kalantar-Zadeh, *J. Mater. Chem. C*, 2 (2014) 5247.
24. M. Izaki, M. Nagai, K. Maeda, F.B. Mohamad, K. Motomura, J. Sasano, T. Shinagawa, S. Watase, *J. Electrochem. Soc.*, 158 (2011) D578.
25. M.J. Siegfried, K.S. Choi, *Adv. Mater.*, 16 (2004) 1743.
26. Y. Yang, Y. Li, M. Pritzker, *Electrochim. Acta*, 213 (2016) 225.
27. I.G. Casella, M. Gatta, *J. Electroanal. Chem.*, 494 (2000) 12.
28. P. Poizot, C.J. Hung, M.P. Nikiforov, E.W. Bohannan, J.A. Switzer, *Electrochem. Solid-State Lett.*, 6 (2003) 2.
29. M.J. Siegfried, K.S. Choi, *Angew. Chem., Int. Ed.*, 44 (2005) 3218.
30. J. Sasano, K. Motomura, M. Nagai, F.B. Mohamad, M. Izaki, *Electrochemistry*, 79 (2011) 831.
31. R. Vittal, K.C. Ho, *Catal. Rev.: Sci. Eng.*, 57 (2015) 145.

32. I.G. Casella, *J. Electroanal. Chem.*, 520 (2002) 119.
33. A. Noorbakhsh, M.M. Mirkalaei, M.H. Yousefi, S. Manochehri, *Electroanalysis*, 26 (2014) 2716.
34. S.K. Meher, G.R. Rao, *Nanoscale*, 5 (2013) 2089.
35. T.N. Huan, G. Rousse, S. Zanna, I.T. Lucas, X. Xu, N. Menguy, V. Mougel, M. Fontecave, *Angew. Chem., Int. Ed.*, 56 (2017) 4792.
36. Z. Zhang, W. Hu, Y. Deng, C. Zhong, H. Wang, Y. Wu, L. Liu, *Mater. Res. Bull.*, 47 (2012) 2561.
37. Y. Yang, J. Han, X. Ning, W. Cao, W. Xu, L. Guo, *ACS Appl. Mater. Interfaces*, 6 (2014) 22534.
38. D. Grujicic, B. Pesic, *Electrochim. Acta*, 47 (2002) 2901.
39. W. Xu, S. Dai, X. Wang, X. He, M. Wang, Y. Xi, C. Hu, *J. Mater. Chem. B*, 3 (2015) 5777.
40. J.T.C. Barragan, S. Kogikoski, E.T.S.G. Da Silva, L.T. Kubota, *Anal. Chem.*, 90 (2018) 3357.
41. R.S. Nicholson, I. Shain, *Anal. Chem.*, 36 (1964) 706.
42. P.J.M. Isherwood, J.M. Walls, *Energy Procedia*, 60 (2014) 129.
43. M. Nolan, S.D. Elliott, *Phys. Chem. Chem. Phys.*, 8 (2006) 5350.
44. S.L. Moura, R.R. De Moraes, M.A.P. Dos Santos, D.D.L. Moreira, J.A.D. Lopes, M.I. Pividori, V. Zucolotto, J.R.D.S. Júnior, *Sens. Actuators, B*, 202 (2014) 469.
45. J. Preza de la Vega, Estudio Electroquímico Aplicado a La Cuantificación de Azúcares En Mieles, Facultad de Química, UNAM, 2007.
46. C.M. Wong, K.H. Wong, X.D. Chen, *Appl. Microbiol. Biotechnol.*, 78 (2008) 927.
47. K. Cao, H. Zhang, Z. Gao, Y. Liu, Y. Jia, H. Liu, *New J. Chem.*, 44 (2020) 18449.
48. E.J. Hoorn, *J. Nephrol.*, 30 (2017) 485.
49. I. Puigdomenech, "Hydra logK Database", can be found under <https://www.kth.se/che/medusa/>
50. A.R. Alonso-Gómez, Electroseparación Selectiva de Plata a Partir de Soluciones Amoniacales de Tiosulfato, Universidad Autónoma Metropolitana-Iztapalapa, 2007.
51. F. Burriel Martí, S. Arribas Jimeno, F. Lucena Conde, J. Hernández Méndez, *Química Analítica Cualitativa*, 18th ed., Thomson, (2003) Spain.
52. M. Pourbaix, Atlas of Electrochemical Equilibria in Aqueous Solutions, 2nd ed., National Association of Corrosion Engineers, (1974) USA.
53. J. Chivot, L. Mendoza, C. Mansour, T. Pauporté, M. Cassir, *Corros. Sci.*, 50 (2008) 62.
54. Mettler-Toledo, "D-Glucose Density concentration table (+20°C)", can be found under https://www.mt.com/ch/en/home/supportive_content/concentration-tables-ana/D_Glucose_de_e.html